Equilibrium ternary intermetallic phase in the Mg–Zn–Ca system

Jake D. Cao
Laboratory of Metal Physics and Technology, Department of Materials, ETH Zurich, 8093 Zurich, Switzerland
Thomas Weber
Laboratory of Crystallography, Department of Materials, ETH Zurich, 8093 Zurich, Switzerland
Robin Schäublin and Jörg F. Löffler[a),b)]
Laboratory of Metal Physics and Technology, Department of Materials, ETH Zurich, 8093 Zurich, Switzerland

(Received 7 October 2015; accepted 2 May 2016)

This study investigates the ternary intermetallic phases in the Mg–Zn–Ca system, which is of great interest for metallic biodegradable implant applications. According to published phase diagrams, the key alloy composition studied herein is located within the $Ca_2Mg_5Zn_5$, $Ca_2Mg_6Zn_3$, and IM1 phase fields. Through controlled cooling of the melt, a quasibinary ~$Ca_2Mg_5Zn_5$–Mg microstructure was obtained. The large polygonal grains had a composition of $Ca_2Mg_5Zn_5$ as determined by energy-dispersive x-ray spectroscopy (EDX). Differential scanning calorimetry revealed that $Ca_2Mg_5Zn_5$ begins to form at ~417 °C, and the eutectic temperature is ~369 °C. Based on single-crystal x-ray diffraction data, $Ca_2Mg_5Zn_5$ was determined to be hexagonal ($P6_3/mmc$), with lattice parameters of a = 9.5949(3) Å and c = 10.0344(3) Å. This was also verified by transmission electron microscopy. Further refinements, which considered the possibility of mixed Mg/Zn sites, significantly improved the data fit compared to the initial ordered structural model. The final refined structure possesses a composition of $Ca_{16}Mg_{42}Zn_{42}$, very similar to the chemical analysis results from EDX.

I. INTRODUCTION

Development of new metallic biomaterials has traditionally focused on improving their longevity. Recent trends observed a paradigm shift, with absorbable metallic alloys intentionally designed to degrade inside the human body over time.[1–4] Notable research on the Mg–Zn–Ca ternary system[5–12] showed promise for this system's deployment as temporary implant material and has attracted the attention of both the research community and industry. One of the challenges in this context is to simultaneously achieve high strength and high ductility in these absorbable alloys. Here fine-grained microstructures with grain sizes in the micron range were shown to be ideal for magnesium-based alloys,[13–15] as this enables Hall–Petch strengthening while allowing for nonbasal slip and grain-boundary sliding. Fine-grained Mg alloys have also been reported to degrade slower in biocorrosion environments.[16,17] As such, a strategy to engineer second-phase particles to pin the grain boundaries during thermomechanical processing has exhibited up to 27% elongation to fracture and up to 240 MPa yield strength.[6] For any alloy design strategy based on intermetallic phases, a reliable phase diagram in the parent system is critical because it would underpin alloy design and processing optimization to achieve the desired properties.

Interestingly, for the Mg–Zn–Ca alloy system there appears to be a lack of understanding with regard to the existence and confirmation of the ternary intermetallic phase/s. The earliest work on the Mg–Zn–Ca system was performed in 1934 by Paris,[18] who produced 215 alloys within this system, 187 of which were ternary alloys. A "large polygonal" ternary phase with a composition of $Ca_2Mg_5Zn_5$ was reported. In 1961 Clark[19] prepared 76 key alloys in the Mg–Zn–Ca system through casting and subsequent heat treatment at 335 °C. Clark did not observe the $Ca_2Mg_5Zn_5$ phase, but instead reported two new ternary phases: (β) $Ca_2Mg_6Zn_3$ and (ω) $Ca_2Mg_5Zn_{13}$. The diffraction data accompanying these two new ternary phases were filed with the Joint Committee on Powder Diffraction Standards [12-0266 (Ref. 20) and 12-569 (Ref. 21)], but no structural data were reported.

Recent efforts by Larionova et al.[22] in 2001 and Jardim et al.[23,24] in 2002 claimed to have confirmed the existence of this β $Ca_2Mg_6Zn_3$ phase. Larionova[22] aimed to develop magnesium alloys for high-temperature structural applications, where melt-spun ribbons of Mg–Zn–Ca alloys with up to 4.25 at.% of Zn and up to 3.19 at.% of Ca were produced. The identification of the ternary intermetallic phase was based on x-ray diffraction (XRD)

Contributing Editor: Yang-T. Cheng
[a)]Address all correspondence to this author.
e-mail: joerg.loeffler@mat.ethz.ch
[b)]This author was an editor of this journal during the review and decision stage. For the *JMR* policy on review and publication of manuscripts authored by editors, please refer to http://www.mrs.org/jmr-editor-manuscripts/.
DOI: 10.1557/jmr.2016.196

 © Materials Research Society 2016

https://doi.org/10.1557/jmr.2016.196 Published online by Cambridge University Press

peaks which were found to closely match the peak positions of the reference data for the $Ca_2Mg_6Zn_3$ phase reported by Clark.[20] Jardim et al.[23,24] intended to characterize the crystallographic structure of the ternary phase in question. Because it became evident that XRD did not provide sufficient signal to reliably identify the phases in their melt-spun ribbon (Mg–1.5Ca–6Zn), transmission electron microscopy (TEM)-based techniques were subsequently applied. This approach was undermined by a critical assumption: TEM energy-dispersive x-ray spectroscopy (EDX) analysis observed a ternary phase with a composition of $Ca_{23.2\pm1}Mg_{43.8\pm3.3}Zn_{33\pm2.4}$, which is roughly equivalent to $Ca_2Mg_4Zn_3$. However, this ternary phase was identified as $Ca_2Mg_6Zn_3$, based on the assumption that "the closest compound found in the literature was $Ca_2Mg_6Zn_3$".[23] Numerous researchers have since come to similar conclusions based on the same assumption that $Ca_2Mg_6Zn_3$ is the most common ternary phase.[8,16,25,26] Critical analysis of these publications revealed that the work by Clark[19] had an immense influence on the outcomes of later research concerning identification of the ternary phase as $Ca_2Mg_6Zn_3$.

Most recently, work of Zhang et al.[27–29] suggested the existence of four intermetallics, IM1-4 (Table I). These were derived through a series of experiments involving 9 diffusion couples and 32 key samples in the Mg–Zn–Ca ternary system. Analysis of 6 key alloys [green triangles in Fig. 1(b)] observed extended solid solubility ranges in IM1. The impact of Zhang's work is significant, because the composition range of the proclaimed IM1 encompasses both that of $Ca_2Mg_5Zn_5$ and $Ca_2Mg_6Zn_3$.

The works of Clark[19] and Zhang[30] set out specifically to investigate the thermodynamic phase equilibria in the Ca–Mg–Zn ternary system, and are essential to our current understanding of this system. It is worth noting, however, that their analyses were based on experimental data collected from samples at 335 °C only. Samples from Clark[19] were cast, then heat-treated at 335 °C for 500 h, and Zhang[30] prepared numerous diffusion couples by heat treatment at 335 °C for 4 wk. Nevertheless, no consensus has been reached regarding the composition of the ternary equilibrium Mg–Zn–Ca intermetallic phase.

In the present work we produced a ternary alloy of composition $Mg_{58.15}Zn_{29.45}Ca_{12.40}$, by controlled cooling of the melt using a gradient Bridgman setup. The very slow cooling rate achieved by this method, coupled with stable temperature control, can approximate equilibrium cooling conditions. Thus, this method produced an equilibrium microstructure consisting of large polygonal grains, which were analyzed using electron microscopy, EDX, and both single-crystal and powder XRD. Below we report on the crystal structure, composition, and diffraction pattern of the resulting ternary Mg–Zn–Ca intermetallic phase.

TABLE I. Intermetallic phases IM1-4, reported by Zhang et al.[28]

Intermetallic designation	Chemical formulae	
IM1	$Ca_3Mg_xZn_{15-x}$	($4.6 \le x \le 12$ at 335 °C)
IM2	$Ca_{14.5}Mg_{15.8}Zn_{69.7}$	...
IM3	$Ca_xMg_yZn_z$	($8.2 \le x \le 9.1$; $27.1 \le y \le 31.0$; $60.8 \le z \le 64$)
IM4	$Ca_{1.5}Mg_{55.3}Zn_{43.2}$	...

II. EXPERIMENTAL METHODS

To allow sufficient time for grain growth, slow and controlled cooling was achieved using a gradient Bridgman induction furnace. The alloy with a nominal composition of 12.40 at.% Ca, 58.15 at.% Mg, and 29.45 at.% Zn (marked as a red star in Fig. 1) was produced first by melting the constituent elements, Mg (99.99 wt% purity, ChemCo GmbH, Bad Soden-Salmünster, Germany), Zn (99.99 wt%, Alfa Aesar GmbH, Karlsruhe, Germany), and Ca (97 wt%, Alfa Aesar GmbH), within a graphite crucible in an induction oven, followed by gravity copper mold casting. All steps were performed under inert argon atmosphere (6 N purity). Specimens of the as-cast sample were analyzed via differential scanning calorimetry (DSC 220C, Seiko Instruments GmbH, Neuisenburg, Germany), using heating and cooling rates of 10 K/min, to detect the associated phase transitions. The remaining as-cast rod was then placed into another graphite crucible, with an iron initiator located at the bottom. The combined vessel was sealed in a quartz tube under argon, and the sample was allowed to grow vertically in the gradient Bridgman setup. The upper and lower ends of the temperature gradient were selected as 600 °C and 335 °C, respectively, and a growth speed of 1 mm/h was chosen. This produced the first phases to precipitate from the melt in sufficiently large grain sizes. Phase compositions were determined using EDX elemental analyses via both scanning electron microscopy (SEM; Hitachi SU-70, Hitachi Corp., Tokyo, Japan), sampling multiple grains, and transmission electron microscopy (TEM; FEI Tecnai F30, FEI Company, Hillsboro, Oregon). XRD experiments were carried out on powder samples (STADI diffractometer, Stoe GmbH, Darmstadt, Germany; Debye-Scherrer geometry; position-sensitive detector; Cu-$K_{\alpha1}$ radiation) and on large single grains (Xcalibur, Oxford Diffraction, Oxford, United Kingdom; Onyx charge-coupled device detector; MoK_α radiation) to characterize the ternary intermetallic crystal structure. Selected area diffraction patterns (SADPs) were obtained using an FEI Talos F200A (FEI Company) operated at 80 kV to minimize beam damage. The SADPs were matched against those simulated by jEMS software,[31,32] based on the proposed crystal unit cell.

https://doi.org/10.1557/jmr.2016.196 Published online by Cambridge University Press

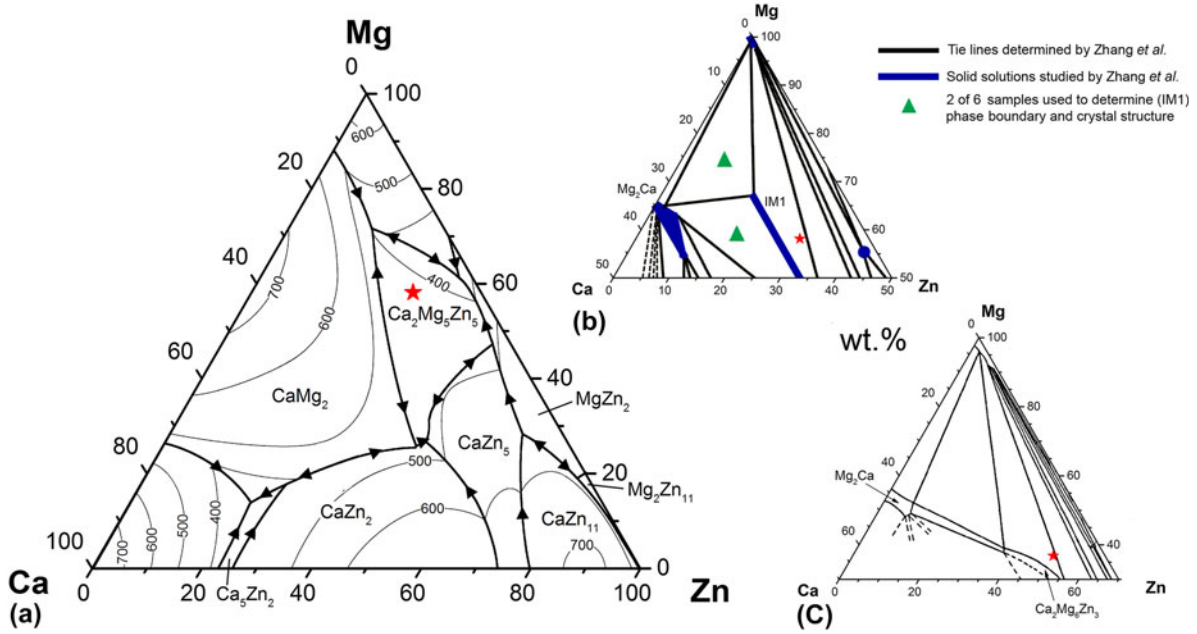


FIG. 1. The key alloy composition (12.40 at.% Ca, 58.15 at.% Mg, and 29.45 at.% Zn), red star, marked in the Mg–Zn–Ca ternary phase diagram published by (a) Villars (based on the data of Paris[18]); (b) Zhang (335 °C isothermal sections)[30]; and (c) Clark[19] (in wt%). According to these reports, the selected key alloy composition (red star) would be located within three different phase fields.

III. RESULTS AND DISCUSSION

Figure 1 shows the nominal composition of the alloy studied relative to the phase fields determined in the literature; based on this, the key alloy composition chosen in this study falls within the $Ca_2Mg_5Zn_5$, $Ca_2Mg_6Zn_3$, and IM1 phase fields according to the respective Mg–Zn–Ca phase diagrams published by Paris,[18] Clark,[19] and Zhang.[30] Newer Mg–Zn–Ca phase diagrams do exist,[33–35] but these were derived via computational optimizations based on the experimental data of Paris, Clark, and Zhang. Thus only those experimental phase diagrams are shown in Fig. 1. DSC analysis from 150 to 650 °C (Fig. 2) revealed three distinct exothermic peaks, which were expected to be, in decreasing order, the liquidus temperature, the eutectic temperature where the ternary phase–Mg lamellae begin to form, and the eutectoid transformation temperature of $Mg_7Zn_3 \rightarrow MgZn + Mg$.[19,36] The determined liquidus temperature of 417 °C is in line with the value compiled by Villars,[37] which is largely based on the work of Paris,[18] and is also similar to the 400 °C determined through thermal analysis during solidification of Mg–0.5Ca–*x*Zn (x = 0.5, 1 and 3).[8] Most critically, the DSC analysis reveals that obvious phase transitions occur at temperatures above 335 °C. This observation supports past studies by Zhang[28,38] and Clark,[19] which used diffusion couples annealed at 335 °C to explore the ternary Mg–Zn–Ca equilibrium phase diagram. At higher annealing temperatures, a liquid phase may exist (see eutectic temperature determined in Fig. 2) which would complicate the interpretation of the diffusion couple experiments.[39]

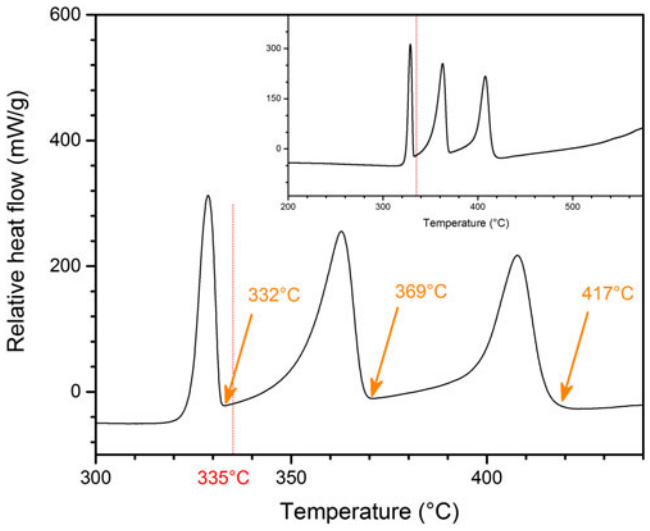


FIG. 2. Representative DSC cooling curve at a rate of 10 K/min for $Mg_{58.15}Zn_{29.45}Ca_{12.40}$, showing distinct exothermic peaks with onsets at 417, 369, and 332 °C. The inset illustrates that the peaks shown were the only exothermic events throughout the temperature range.

Microstructural analysis identified the phase transitions associated with each exothermic peak in the DSC trace. Using upper and lower temperatures of 600 °C and 335 °C, respectively, the gradient Bridgman method produced a rod sample with large polygonal crystals of between ~100 and 500 μm in size that formed a quasibinary with the α-Mg matrix (Fig. 3). Thus the two high-temperature exothermic peaks in Fig. 2 were determined as the liquidus and eutectic temperatures. A selected area

https://doi.org/10.1557/jmr.2016.196 Published online by Cambridge University Press

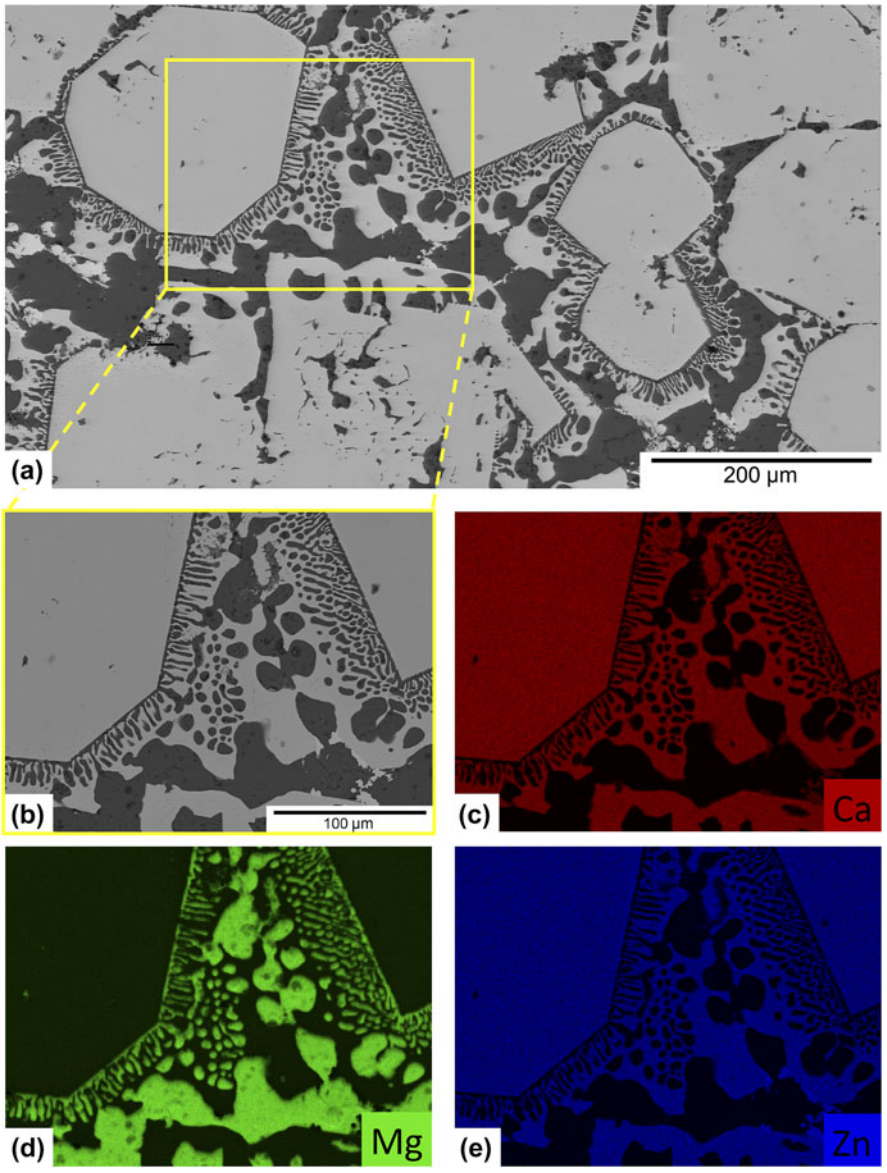


FIG. 3. (a) BSE image obtained from SEM. (b) Magnified area of image (a), on which elemental mapping was performed to investigate (c) Ca, (d) Mg, and (e) Zn.

was subsequently mapped using EDX [Figs. 3(c)–3(e)], which confirmed that the large polygonal grains (bright phase) in the backscattered electron (BSE) image is the ternary intermetallic, and the dark phase in the BSE image is Mg (with Zn in solid solution). A number of additional grains were selected throughout the sample and analyzed by both SEM and TEM EDX to determine their compositions. All of these readings were consistent throughout the sample, and are tabulated including statistics in Table II. Despite the slightly higher Mg value in SEM EDX and the slightly higher Zn value in TEM EDX, these data show similar atomic concentrations of Mg and Zn, resulting in stoichiometric ratios of $\sim Ca_2Mg_5Zn_5$. We therefore refer to this phase as $Ca_2Mg_5Zn_5$. The Zn content in α-Mg is approximately 2.42 at.% (averaged from 5 SEM EDX readings), which is very close to the 2.4 at.% reported as the maximum solid solubility of Zn in Mg at 340 °C.[37]

TABLE II. EDX SEM and EDX TEM elemental analysis of the grains within the $Mg_{58.15}Zn_{29.45}Ca_{12.40}$ sample prepared; n gives the number of measurements that generated a mean value with standard deviation (SD). All values are given in at.%.

	SEM (n = 13)			TEM (n = 3)		
Elements	Ca	Mg	Zn	Ca	Mg	Zn
Mean	14.1	43.6	38.0	15.93	40.01	44.05
SD	0.234	0.850	0.782	1.64	1.94	1.61
Stoichiometric ratio	2.0	6.2	5.4	2.0	5.0	5.5

https://doi.org/10.1557/jmr.2016.196 Published online by Cambridge University Press

It is worth emphasizing that no significant composition difference was observed across the individual grains. Although this work did not establish the solubility limits of $Ca_2Mg_5Zn_5$, work by Zhang[28,30,38] suggested that the Zn and Mg contents in IM1 $Ca_3Mg_xZn_{15-x}$ ($4.6 \leq x \leq 12$ at 335 °C) could each vary by up to 41.1 at.%, thus making $Ca_2Mg_5Zn_5$ a possible variation of IM1 (when $x = 7.5$, IM1 = $Ca_3Mg_{7.5}Zn_{7.5}$ or $Ca_2Mg_5Zn_5$). This observed difference was attributed to sample preparation methods, whereby the current method produced the equilibrium microstructure at 335 °C by controlled cooling of the alloy from its liquid state. The failure to obtain $Ca_2Mg_5Zn_5$ using diffusion couple experiments reaffirmed the known limitations of such methods, where the absence of certain phases may be due to difficulties in nucleation, or quasiequilibrated diffusion zones may have formed instead of the real equilibrium phase.[39]

Microstructural analysis of the current study revealed large polygonal grains of $Ca_2Mg_5Zn_5$ and eutectic ($Ca_2Mg_5Zn_5$ + Mg) lamellae. According to Zhang,[28] the same alloy composition would also generate a microstructure consisting of IM1 (encompassing $Ca_2Mg_5Zn_5$) + Mg. Distinctions must be made between these claims, and we therefore utilize the refined crystal structure parameters. Rietveld refinement of the XRD patterns for IM1[28] showed that this solid solution crystallizes in a hexagonal structure having a $P6_3/mmc$ (194) space group with $Sc_3Ni_{11}Si_4$ prototype. These data should, however, be viewed with caution, as the suggested structure model had an increasingly worsening reliability factor, starting with R_{wp} = 15.8% (for IM1 = $Ca_3Mg_{12}Zn_3$) and reaching 20.5% (for IM1 = $Ca_3Mg_{7.8}Zn_{7.2}$) and 19.6% (for IM1 = $Ca_3Mg_{7.6}Zn_{7.4}$)[28]; the latter two IM1 compositions are very close to ~$Ca_2Mg_5Zn_5$. Due to the poor structural fit, we thus carried out our own structure determination plus refinement work.

The crystal structure of $Ca_2Mg_5Zn_5$ was determined using single-crystal XRD methods. Six large grains of ~100 μm in size were mechanically removed from the bulk sample and measured, and only the data from the highest quality grain was used in the later refinement steps. $Ca_2Mg_5Zn_5$ was found to be hexagonal with lattice parameters of a = 9.5949(3) Å, c = 10.0344(3) Å, and space group $P6_3/mmc$. Structure solution and refinement were solved from scratch with direct methods using the SHELX97 software package.[40] Results are shown in Table III [further details of the crystal structure investigation(s) may be obtained from FIZ Karlsruhe, 76344 Eggenstein-Leopoldshafen, Germany (fax: (+49) 7247-808-666; e-mail: crysdata@fiz-karlsruhe.de, on quoting the deposition number CSD-429847)]. The solved structure can be described as an $Sc_3Ni_{11}Si_4$ type, as already reported in the literature,[28] but with additional Zn atoms, Zn(5) (see Fig. 4), at the symmetry-related sites (0,0,0) and (0,0,0.5). While the past investigation used powder

TABLE III. List of (a) atomic coordinates and occupancies; and (b) ADPs from the single-crystal refinement of $Ca_2Mg_5Zn_5$, where $U_{eq} = \frac{1}{3}\left\langle |\mathbf{u}|^2 \right\rangle$ is the equivalent isotropic displacement parameter, **u** describes the instantaneous displacement, and U_{ij} are the respective elements of the mean-square displacement tensor.

(a)

	x	y	z	Occ.	U_{eq} [Å^2]
Zn(1)	0.5	0	0	1	0.026(1)
Zn(2) Mg(2)	0.4336(1)	0.5664(1)	−0.25	0.758(8) 0.242(8)	0.021(1)
Zn(3) Mg(3)	0.3333	0.6667	−0.0034(2)	0.430(9) 0.570(9)	0.022(1)
Zn(4)	0	0	−0.25	0.81(1)	0.026(1)
Zn(5)	0	0	0	0.901(8)	0.025(1)
Mg(6)	0.1600(1)	0.3200(2)	0.5911(2)	1	0.021(1)
Ca(7)	0.2010(1)	0.4021(2)	0.25	1	0.021(1)

(b)

	U_{11} [Å^2]	U_{22} [Å^2]	U_{33} [Å^2]	U_{23} [Å^2]	U_{13} [Å^2]	U_{12} [Å^2]
Zn(1)	0.0218(4)	0.0241(5)	0.0342(6)	−0.0106(3)	−0.0053(2)	0.0120(3)
Zn(2) Mg(2)	0.0211(5)	0.0211(5)	0.0190(6)	0	0	0.0096(4)
Zn(3) Mg(3)	0.0203(7)	0.0203(7)	0.0258(10)	0	0	0.0102(3)
Zn(4)	0.0254(8)	0.0254(8)	0.0281(12)	0	0	0.0127(4)
Zn(5)	0.0217(7)	0.0217(7)	0.0304(11)	0	0	0.0108(3)
Mg(6)	0.0198(7)	0.0214(9)	0.0213(9)	−0.0011(6)	−0.0005(3)	0.0107(4)
Ca(7)	0.0213(6)	0.0226(8)	0.0206(7)	0	0	0.0113(4)

https://doi.org/10.1557/jmr.2016.196 Published online by Cambridge University Press

XRD[28] with the assumption of a $Sc_3Ni_{11}Si_4$ prototype, the structure in this study was solved from single crystals with no prior assumptions. The initially ordered model showed unsatisfactory *R*-values and unusual large atomic displacement parameters (ADPs) for the Zn atoms, which indicated the presence of disorder. Because Mg and Zn may replace each other due to their similar bond distances,[41] the possibility of mixed Mg/Zn sites was considered for all Zn and Mg positions. The refinement results, however, clearly indicated the absence of any substitutional or occupational disorder for Zn(1) and Mg(6). For Zn(4) and Zn(5) the possibility of mixed occupied Mg/Zn sites was deemed unreasonable because their interatomic distance is only 2.51 Å, which is very short even for Zn–Zn pairs. Substitution of Zn by larger Mg atoms was therefore ruled out and only under-occupied Zn was examined for these sites. For Zn(2)/Mg(2) and Zn(3)/Mg(3) mixed parameters could be successfully modeled. The final disorder model clearly improved the fit: the SHELXL program specific *R*-values[40] dropped from $R1 = 9.0\%$, $wR2 = 28.3\%$ for the initial ordered model to $R1 = 4.8\%$, $wR2 = 9.7\%$. The ADPs of the Zn atoms are still relatively large, but this can be easily explained by size-effect distortions caused by substitutional or occupational disorder. The refined composition of the structure is $Ca_{16.0}Mg_{42.0}Zn_{42.0}$, which is very close to the findings obtained by EDX (Table II).

Powder XRD was carried out to test whether the selected grain for the single-crystal structure refinement was representative of the bulk sample. Approximately 5 g of the sample was ground into fine powder, and underwent XRD scanning from 10 to 90°. Peaks from $Ca_2Mg_5Zn_5$, matched by the lattice parameters determined by the single-crystal x-ray experiment, were found to dominate the diffraction pattern. Reflections from elemental Mg were also identified. Rietveld refinement with a starting model taken from the single-crystal investigation gave a reasonable fit (see Fig. 5) and essentially confirmed the single-crystal results. Furthermore, the lattice parameters and atomic coordinates of $Ca_2Mg_5Zn_5$ from single-crystal and powder refinements differed only by a few 0.01 Å, the site occupation factors agreed within 5%, and the total composition could be reproduced with deviations of less than 1% for each element. The Zn content in the Mg phase was found to be 3.4 at.%, which is also in good agreement with the EDX measurements mentioned above. However, it should be noted that the four shoulders (indicated by arrows in Fig. 5) could not be identified. This may be the result of unidentified phase(s), but considering that these shoulders were only observed near the strongest reflections, and that there were no other unidentified peaks, it is likely that they were caused by strain effects, particle size effects, oxidation of the powder, or a combination of these. The affected volume fraction is estimated to be a few percent. The R_{wp} value of the Rietveld full pattern

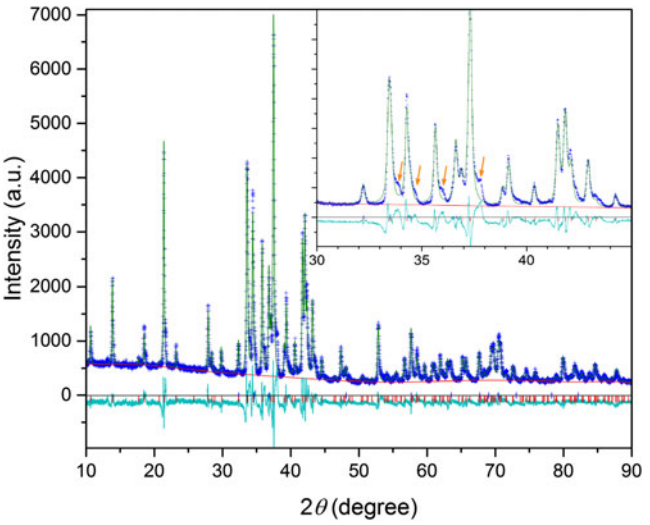


FIG. 5. Results from the Rietveld refinement of the powder sample. Blue symbols: observed (experimental) intensities; green line: calculated intensities; turquoise line: $I_{obs} - I_{calc}$; red line: estimated background. Blue and red markers indicate reflection positions of the two refined phases. Arrows in the inset show some unidentified shoulders which may have resulted from variations in strain and particle size, or minor oxidation of the powder.

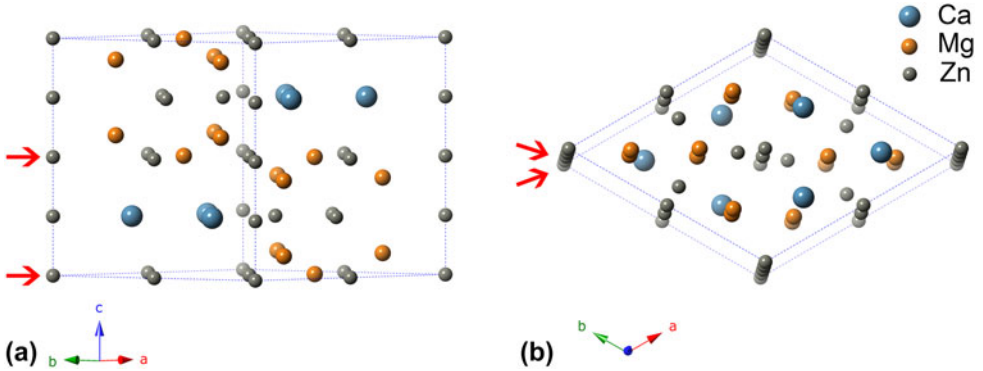


FIG. 4. The crystal structure of $Ca_2Mg_5Zn_5$ as viewed (approximately) along the (a) [110] and (b) [001] directions. Zn atoms not belonging to the $Sc_3Ni_{11}Si_4$ structure type are marked by red arrows.

https://doi.org/10.1557/jmr.2016.196 Published online by Cambridge University Press

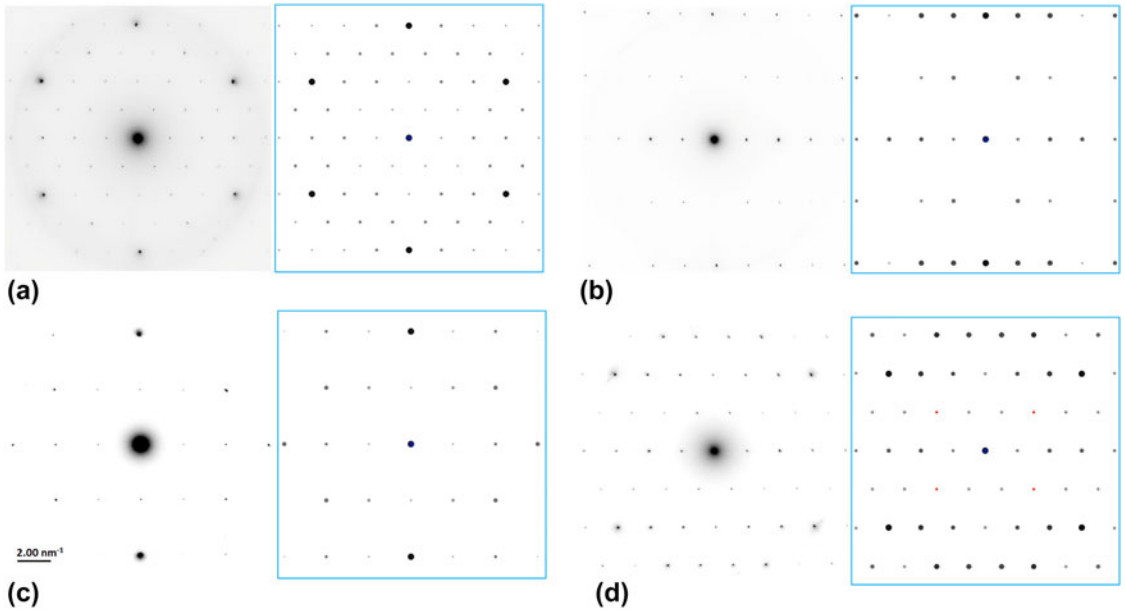


FIG. 6. SADPs, in inverted contrast, of $Ca_2Mg_5Zn_5$ crystals observed in the key alloy $Ca_{12.40}Mg_{58.15}Zn_{29.45}$. Four different crystallographic directions are shown: (a) [0001], (b) $[2\bar{1}\bar{1}6]$, (c) $[10\bar{1}2]$, and (d) $[2\bar{1}\bar{1}3]$. The experimental SADPs are shown next to their corresponding simulated patterns using jEMS (displayed in blue frames).

fit was 11.3%. It is well-known that powder XRD refinements are less reliable than single-crystal investigations, and that this is particularly true in the presence of disorder and unidentified phases. Therefore we only report single-crystal refinement results here.

Because the structural information on $Ca_2Mg_5Zn_5$ was determined from scratch using single-crystal XRD and reported here for the first time, TEM SADP analysis was performed to match the experimental patterns obtained from the key alloy ($Ca_{12.40}Mg_{58.15}Zn_{29.45}$) with those simulated by jEMS, using the structural information from Table III. Visual comparisons between the experimental and simulated SADPs are presented in Fig. 6, for the zone axes (a) [0001], (b) $[2\bar{1}\bar{1}6]$, (c) $[10\bar{1}2]$, and (d) $[2\bar{1}\bar{1}3]$. Note that images are presented in inverted contrast for better readability and that the size of the diffraction spots in the simulated patterns is proportional to their intensity. There appears to be an excellent match between the experimental and simulated patterns for all zone axes considered, confirming the identification of the new phase obtained from XRD. In Fig. 6(d), double diffraction from the Mg matrix and $Ca_2Mg_5Zn_5$ was considered, where the red diffraction spots in the simulated pattern resulted from the Mg matrix. When viewed together with the diffraction pattern of $Ca_2Mg_5Zn_5$, there was also good agreement between the experimental and simulated patterns thus confirming the derived structure for $Ca_2Mg_5Zn_5$.

The experimentally obtained ternary phase from equilibrium cooling, $Ca_2Mg_5Zn_5$, and the subsequent refinement of its structure may have a profound impact on our understanding of the Mg–Zn–Ca system, which has largely been based on thermodynamic calculations. For example, the computational thermodynamic model developed by Brubaker and Liu[33] abandoned $Ca_2Mg_5Zn_5$ and assumed $Ca_2Mg_6Zn_3$ to be the only ternary intermetallic phase in the system. Alternative CALPHAD models[34,35] considered up to four different ternary phases. In light of the new experimental data reported here, further CALPHAD optimization studies are suggested to determine the potential impact of the $Ca_2Mg_5Zn_5$ ternary intermetallic phase on the calculated Mg–Zn–Ca ternary system. This may also have important consequences for the development of new high strength, highly ductile, and biodegradable MgZnCa alloys.[6]

IV. SUMMARY

A ternary Mg–Zn–Ca alloy with 12.40 at.% Ca, 58.15 at.% Mg, and 29.45 at.% Zn was successfully synthesized by controlled cooling of the melt, with its composition deliberately chosen to lie within various disputed phase fields. Microstructural analysis revealed large polygonal grains determined by EDX to be $Ca_2Mg_5Zn_5$, which appears to exist as a quasibinary with α-Mg. DSC suggests that this ternary phase forms at ~417 °C, and XRD determined the $Ca_2Mg_5Zn_5$ phase to be of hexagonal structure, space group $P6_3/mmc$, with lattice parameters of a = 9.5949(3) Å and c = 10.0344(3) Å. Parametric refinement clearly improved the data fit, resulting in a composition of $Ca_{16.0}Mg_{42.0}Zn_{42.0}$, very close to the $Ca_2Mg_5Zn_5$ reported. TEM (SADP) also confirmed the derived structure for $Ca_2Mg_5Zn_5$.

https://doi.org/10.1557/jmr.2016.196 Published online by Cambridge University Press

ACKNOWLEDGMENTS

The authors thank Erwin Fischer (LMPT, ETH Zurich) for help with the sample preparation, Peter Uggowitzer (LMPT, ETH Zurich) for fruitful discussions, and Fiodar Kurdzesau (Laboratory of Crystallography, ETH Zurich) for performing the single-crystal x-ray measurements. This work was funded by the Laura Bassi Center of Expertise (BRIC, Bioresorbable Implants for Children), FFG, Austria, and by an ETH Research Grant (ETH-41 13-2).

REFERENCES

1. M.P. Staiger, A.M. Pietak, J. Huadmai, and G. Dias: Magnesium and its alloys as orthopedic biomaterials: A review. *Biomaterials* **27**, 1728–1734 (2005).
2. F. Witte, V. Kaese, H. Haferkamp, E. Switzer, A. Meyer-Lindenberg, C.J. Wirth, and H. Windhagen: In vivo corrosion of four magnesium alloys and the associated bone response. *Biomaterials* **26**, 3557–3563 (2005).
3. A.C. Hänzi, I. Gerber, M. Schinhammer, J.F. Löffler, and P.J. Uggowitzer: On the in vitro and in vivo degradation performance and biological response of new biodegradable Mg–Y–Zn alloys. *Acta Biomater.* **6**, 1824–2833 (2010).
4. T. Kraus, S.F. Fischerauer, A.C. Hänzi, P.J. Uggowitzer, J.F. Löffler, and A.M. Weinberg: Magnesium alloys for temporary implants in osteosynthesis: In-vivo studies of their degradation and interaction with bone. *Acta Biomater.* **8**, 1230–1238 (2012).
5. B. Zberg, P.J. Uggowitzer, and J.F. Löffler: MgZnCa glasses without clinically observable hydrogen evolution for biodegradable implants. *Nat. Mater.* **8**, 887–891 (2009).
6. J. Hofstetter, M. Becker, E. Martinelli, A.M. Weinberg, B. Mingler, H. Kilian, S. Pogatscher, P.J. Uggowitzer, and J.F. Löffler: High-strength low-alloy (HSLA) Mg–Zn–Ca alloys with excellent biodegradation performance. *JOM* **66**, 566–572 (2014).
7. J. Hofstetter, E. Martinelli, S. Pogatscher, P. Schmutz, E. Povoden-Karadeniz, A.M. Weinberg, P.J. Uggowitzer, and J.F. Löffler: Influence of trace impurities on the in vitro and in vivo degradation of biodegradable Mg–5Zn–0.3Ca alloys. *Acta Biomater.* **23**, 347–353 (2015).
8. H.R. Bakhsheshi-Rad, M.R. Abdul-Kadir, M.H. Idris, and S. Farahany: Relationship between the corrosion behavior and the thermal characteristics and microstructure of Mg–0.5Ca–*x*Zn alloys. *Corros. Sci.* **64**, 184–197 (2012).
9. H.R. Bakhsheshi-Rad, E. Hamzah, A. Fereidouni-Lotfabadi, M. Daroonparvar, M.A.M. Yajid, M. Mezbahul-Islam, M. Kasiri-Asgarani, and M. Medraj: Microstructure and bio-corrosion behavior of Mg–Zn and Mg–Zn–Ca alloys for biomedical applications. *Mater. Corros.* **65**, 1178–1187 (2014).
10. K. Hagihara, S. Shakudo, K. Fujii, and T. Nakano: Degradation behavior of Ca–Mg–Zn intermetallic compounds for use as biodegradable implant materials. *Mater. Sci. Eng., C* **44**, 285–292 (2014).
11. X. Gu, Y. Zheng, S. Zhong, T. Xi, J. Wang, and W. Wang: Corrosion of, and cellular responses to Mg–Zn–Ca bulk metallic glasses. *Biomaterials* **31**, 1093–1103 (2010).
12. X. Xie, X. Wang, Y. Wang, G. Zhang, Y. He, Y. Zheng, and L. Qin: Ca–Mg–Zn metallic glass as degradable biomaterials developed for potential orthopaedic applications. *Bone* **47**, 425 (2010).
13. A.C. Hänzi, A.S. Sologubenko, P. Gunde, M. Schinhammer, and P.J. Uggowitzer: Design considerations for achieving simultaneously high-strength and highly ductile magnesium alloys. *Philos. Mag. Lett.* **92**, 417–427 (2012).
14. A.C. Hänzi, F.H. Dalla Torre, A.S. Sologubenko, P. Gunde, R. Schmid-Fetzer, M. Kuehlein, J.F. Löffler, and P.J. Uggowitzer: Design strategy for microalloyed ultra-ductile magnesium alloys. *Philos. Mag. Lett.* **89**, 377–390 (2009).
15. J. Hofstetter, S. Rüedi, I. Baumgartner, H. Kilian, B. Mingler, E. Povoden-Karadeniz, S. Pogatscher, P.J. Uggowitzer, and J.F. Löffler: Processing and microstructure-property relations of high-strength low-alloy (HSLA) Mg–Zn–Ca alloys. *Acta Mater.* **98**, 423–432 (2015).
16. Y. Lu, A.R. Bradshaw, Y.L. Chiu, and I.P. Jones: Effects of secondary phase and grain size on the corrosion of biodegradable Mg–Zn–Ca alloys. *Mater. Sci. Eng., C* **48**, 480–486 (2015).
17. K.D. Ralston and N. Birbilis: Effect of grain size on corrosion: A review. *Corrosion* **66**, 0750051 (2010).
18. R. Paris: Publications scientifiques et techniques du minist'ere de l'air, Ministere de L'Air, 1–86 (1934).
19. J.B. Clark: The solid constitution in the magnesium-rich region of the Mg–Ca–Zn phase diagram. *Trans. Metall. Soc. AIME* **221**, 644–645 (1961).
20. J.B. Clark: *Joint Committee on Powder Diffraction Standards (JCPDS)* Card. 12-266 (1961).
21. J.B. Clark: *Joint Committee on Powder Diffraction Standards (JCPDS)* Card. 12-569 (1961).
22. T.V. Larionova, W-W. Park, and B-S. You: A ternary phase observed in rapidly solidified Mg–Ca–Zn alloys. *Scr. Mater.* **45**, 7–12 (2001).
23. P.M. Jardim, G. Solórzano, and J.B.V. Sande: Precipitate crystal structure determination in melt spun Mg–1.5wt%Ca–6wt%Zn alloy. *Microsc. Microanal.* **8**, 487–496 (2002).
24. P.M. Jardim, G. Solórzano, and J.B.V. Sande: Second phase formation in melt-spun Mg–Ca–Zn alloys. *Mater. Sci. Eng., A* **381**, 196–205 (2004).
25. K. Oh-ishi, R. Watanabe, C.L. Mendis, and K. Hono: Age-hardening response of Mg–0.3 at.% Ca alloys with different Zn contents. *Mater. Sci. Eng., A* **526**, 177–184 (2009).
26. F. Naghdi and R. Mahmudi: Effect of solution treatment on the microstructural evolution and mechanical properties of an aged Mg–4Zn–0.3Ca alloy. *Mater. Sci. Eng., A* **631**, 144–152 (2015).
27. Y-N. Zhang, D. Kevorkov, F. Bridier, and M. Medraj: Morphological and crystallographic characterizations of the Ca–Mg–Zn intermetallics appearing in ternary diffusion couples. *Adv. Mater. Res.* **409**, 387–392 (2012).
28. Y-N. Zhang, D. Kevorkov, J. Li, E. Essadiqi, and M. Medraj: Determination of the solubility range and crystal structure of the Mg-rich ternary compound in the Ca–Mg–Zn system. *Intermetallics* **18**, 2404–2411 (2010).
29. Y-N. Zhang, D. Kevorkov, X.D. Liu, F. Bridier, P. Chartrand, and M. Medraj: Homogeneity range and crystal structure of the $Ca_2Mg_5Zn_{13}$ compound. *J. Alloys. Compd.* **523**, 75–82 (2012).
30. Y-N. Zhang: Experimental investigation of the Ca–Mg–Zn system via diffusion couples and key experiments (thesis); performed at the Department of Mechanical and Industrial Engineering, Concordia University, Montreal, Canada, 2010.
31. P.A. Stadelmann: EMS—A software package for electron-diffraction analysis and HREM image simulation in materials science. *Ultramicroscopy* **21**, 131–145 (1987).
32. "JEMS-SAAS V4", P.A. Stadelmann, 2015, http://www.jems-saas.ch/.
33. C.O. Brubaker and Z-K. Liu: A computational thermodynamic model of the Ca–Mg–Zn system. *J. Alloys. Compd.* **370**, 114–122 (2004).
34. M. Mezbahul-Islam, Y.N. Zhang, C. Shekhar, and M. Medraj: Critical assessment and thermodynamic modeling of Mg–Ca–Zn system supported by key experiments. *CALPHAD* **46**, 134–147 (2014).
35. S. Wasiur-Rahman and M. Medraj: Critical assessment and thermodynamic modeling of the binary Mg–Zn, Ca–Zn and ternary Mg–Ca–Zn systems. *Intermetallics* **17**, 847–864 (2009).

https://doi.org/10.1557/jmr.2016.196 Published online by Cambridge University Press

36. H.O. Thaddeus, B. Massalski, P.R. Subramanian, and L. Kacprzak: Binary alloy phase diagrams. In *Mg–Zn Phase Diagram*, Hugh Baker, ed. (ASM International, Materials Park, Ohio, 1990).
37. P. Villars, A. Prince, and H. Okamoto: *Handbook of Ternary Alloy Phase Diagrams* (ASM International, Materials Park, OH, 1994).
38. Y-N. Zhang, D. Kevorkov, F. Bridier, and M. Medraj: Experimental study of the Ca–Mg–Zn system using diffusion couples and key alloys. *Sci. Technol. Adv. Mater.* **12**, 025003 (2011).
39. A.A. Kodentsov, G.F. Bastin, and F.J.J. van Loo: The diffusion couple technique in phase diagram determination. *J. Alloys. Compd.* **320**, 207–217 (2001).
40. G.M. Sheldrick: A short history of SHELX. *Acta Crystallogr. A* **64**, 112–122 (2007).
41. O.N. Senkov, D.B. Miracle, E.R. Barney, A.C. Hannon, Y.Q. Cheng, and E. Ma: Local atomic structure of Ca–Mg–Zn metallic glasses. *Phys. Rev. B* **82**, 104206 (2010).

https://doi.org/10.1557/jmr.2016.196 Published online by Cambridge University Press